ATMOSPHERIC BREATHING ELECTRIC THRUSTER FOR PLANETARY EXPLORATION

Final Report

Grant No. NNX11AR29G

Period of Performance: September 15, 2011 – September 14, 2012

Prepared By:

Kurt Hohman, Principal Investigator

Busek Co. Inc.

11 Tech Circle

Natick, MA 01760-1023

October 5, 2012

Table of Contents

List of Figures ii
List of Tables iii
PROJECT SUMMARY 1
1.0 BACKGROUND 1
1.1 Hall Effect Thruster Description 3
2.0 Phase I Results 4
2.1 Hall Thruster Model for CO_2 6
2.2 Inlet Evaluation 8
2.3 Concept Evaluation in Realistic Application 10
2.4 Testing and Characterization of Radio Frequency Neutralizer on Carbon Dioxide 15
3.0 Next Steps in Development 28
4.0 Technology Roadmap 33
5.0 Conclusions 35
6.0 References 35

List of Figures

Figure 1 Conceptual MABHET powered vehicle....2
Figure 2 Cross-sectional schematic of a typical Hall thruster with closed electron drift....3
Figure 3 Hall thruster running on CO2 in Busek facility....4
Figure 4 Thrust to power versus anode voltage for Hall thruster running on Mars mixture....5
Figure 5 Thrust to power versus gas flow at various anode voltages for a Hall thruster running on Mars mixture....5
Figure 6 Thrust versus anode voltage for Hall thruster running on Mars mixture....6
Figure 7 Calculated thrust to power versus voltage for Xe (125 eV ion energy cost) and CO_2 (200 ev ion energy cost)....7
Figure 8 Calculated thrust to power for CO_2 at 3 different values of ion energy cost....7
Figure 9 Conceptual diagram of inlet process....9
Figure 10 Density distribution predicted by the DSMC code for a collection tube 60 cm in diameter....9
Figure 11 Collection efficiency predicted by the DSMC code. The density used here is the density of the incoming gas....10
Figure 12 Thrust to counteract drag assuming different drag coefficients....11
Figure 13 Power required to overcome drag at different drag coefficients....12
Figure 14 Collection efficiency required to overcome drag for different drag coefficients....12
Figure 15 Thermal power of particles incident on the spacecraft versus altitude....13
Figure 16 Thermal power radiated versus temperature of radiating surface....13
Figure 17 Schematic Representing Specular and Diffuse Reflection....15
Figure 18 Schematic Representing the CCL Reflection Model....15
Figure 19 Cross section of the RFN (from Plasma Process Group, Inc. - Radio Frequency Neutralizer Manual)....16
Figure 20 RFN electrical diagram (from Plasma Process Group, Inc. - Radio Frequency Neutralizer Manual)....17
Figure 21 Electrical schematic including monitors....17
Figure 22 Busek arcjet operating in free jet mode....29
Figure 23 Busek REFT operating with nitrogen....29
Figure 24 Busek micro-Newton torsion balance....30
Figure 25 Concept sketch of drag measurements....30
Figure 26 Busek's ECR cathode operating on gas mixture that contains CO2....32
Figure 27 Truncated graph of terrestrial photovoltaic advances....34

List of Tables

Table 1 Example of measurements and calculations of accommodation coefficients for sample materials subjected to 5eV AO beam 30

Table 2 Technology Roadmap to Successful Mars Flight 34

PROJECT SUMMARY

The objective of this phase of the program was to show feasibility of a Martian atmosphere breathing Hall effect thruster (MABHET). To accomplish this objective, we set out to demonstrate that: 1) a Busek Hall effect thruster could operate on the Mars atmospheric gases, 2) the atmospheric conditions and orbital parameters required for the MABHET were indeed achievable, 3) further advancement of the inlet concept held credible, and 4) continued investigation into the remaining vehicle components including the cathode, power generation, size/mass and science remained feasible. We achieved all of these goals during the first phase of this program.

One major achievement during this phase was the operation of a Busek HET with simulated Mars atmosphere. Two goals included an overall efficiency of at least 20% and a maximum thrust to power ratio since the vehicle would likely be power limited. The HET was operated over a wide range of mass flow, applied anode voltage and overall power, simulating various potential altitudes and size of the thruster. Definitive thrust measurements prove that 20% efficiency is indeed possible and likely on the low end of expected performance. The thrust to power ratio peaked around 30mN/kW with an efficiency around 22-25%, depending on the operating conditions. This measured performance with be discussed in more detail below.

Sizing of the vehicle, propulsion system and Mars atmosphere conditions also need to be confirmed that such a concept is feasible. The major drivers of this analysis are the vehicle drag and solar flux/collection. Utilizing current technology for spacecraft drag and solar arrays, the MABHET concept is right on the edge of feasibility. However, solar arrays are becoming more efficient on a study pace and drag in rarefied atmospheres is also becoming better understood. Minor improvements, in either or both of these areas, will confirm credibility to MABHET feasibility for future missions.

The atmospheric inlet or propellant collector is a critical component for the MABHET concept to work. We chose to further our investigation of the inlet numerically utilizing DSMC and we found that shrinking the inlet proportionally for a smaller thruster/vehicle design also held performance, thus the focus on a lower power, smaller vehicle was also feasible. The inlet is the lead critical path component and needs to be investigated early in future programs.

Finally, analysis and some experiments on the remaining propulsion system components and spacecraft design were initialized during phase I. This included some radio frequency cathode tests performed by Colorado State University. Though these tests were unsuccessful, rational for the failure and a path to success has been determined. We also began looking at the science made possible by this concept and who in the science community might be interested. Solar array advances and possible low drag surfaces are discussed.

1.0 BACKGROUND

Conceptually the thruster is analogous to a conventional jet engine, except the energy input is not chemical but electrical, converting the low pressure Martian atmosphere into a non-equilibrium plasma and accelerating it rearward by electromagnetic means to create thrust. Such a craft, which is strictly speaking neither aircraft nor spacecraft, could remain in flight around Mars indefinitely, powered by the sun and never exhausting its propellant supply. An artist conceptual sketch of the MABHET powered vehicle is shown in Figure 1. The concept is of course applicable to flight around any planet, including Earth, as long as the planet has a suitable atmosphere and sufficient solar power flux.

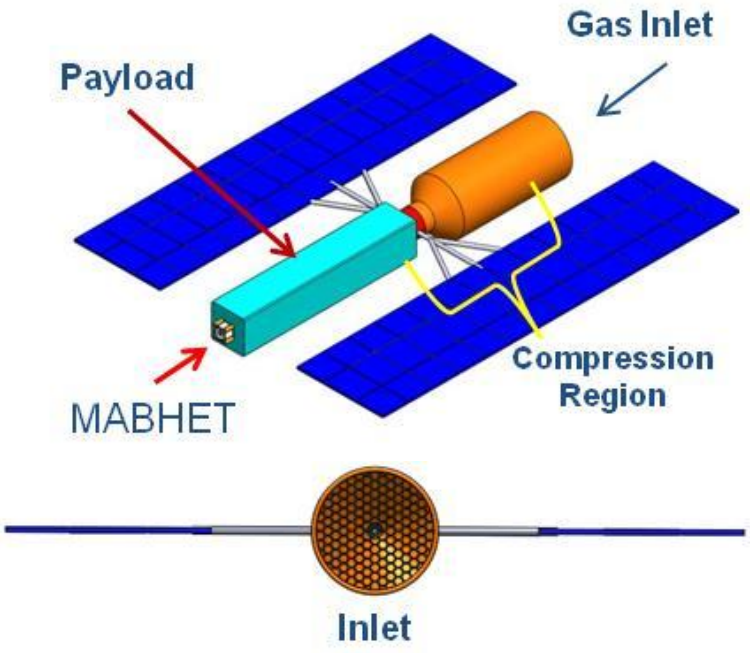

Figure 1 Conceptual MABHET powered vehicle

The Wright brothers flew the world's first successful powered airplane in 1903. In the late 1990s, NASA had planned to fly a powered airplane on Mars in 2003 to commemorate this achievement. The Mars Airplane Package fell short of fruition due to restricted funded and higher priority development[1]. More recently NASA Langley has been developing a liquid rocket powered vehicle for the proposed ARES Mars Scout Mission[2]. Though the ARES has some unique science capabilities, the longest flight duration is just a few hours. In addition, several conceptual aircraft have been described including the solar and radioisotope/heat engine powered planes[3] and lighter-than-air vehicles (dirigibles[4]).

Mars has a very thin atmosphere (about 6 to 7 Torr pressure at ground level) mostly composed of CO_2. While one may consider a powered flight using a specialized fuel reacted with the Martian atmosphere or carry both fuel and oxidizer for short missions, it is much preferable to use electricity derived from solar cells to power such a craft, because it avoids lifting fuel to Mars or synthesizing it in-situ. However, the solar power flux is only about 40% of that on Earth. The combination of a thin atmosphere and reduced solar incidence creates special demands that force the airplane design into either higher speed flight to generate adequate lift or to large lifting surfaces, both leading to increased power requirements due to larger aerodynamic drag (3). An alternative to this approach is a craft that would skim the upper edges of the Martian atmosphere using it for propulsion.

Multiple science missions can be performed by the proposed MABHET. Low altitude orbital observation and in-situ measurements can be achieved. With the addition of batteries, atmospheric dipping can be performed to take measurements at considerably lower altitudes. Measurements include crustal magnetism, atmospheric boundary layer composition, chemistry and dynamics and near-surface water, all measures proposed by ARES for small fraction of Mars surface. The key differential is that the MABHET craft can range the entire planet over many years, sending countless measurements back to earth.

Initial feasibility analysis and experiments prove the concept is within the realm of near term (~10 years) technology development. The analysis indicates that gas collection, spacecraft drag and power acquisition are the three areas of technology that need to be developed. The proposed program objective is to demonstrate feasibility of the inlet gas collection and low drag of the spacecraft. The power generation, most likely very high efficiency solar arrays, is outside the scope of this program and acceptable, since there is appreciable outside funding for their development.

1.1 Hall Effect Thruster Description

Among the most successful on-board satellite electric thrusters is the Hall effect thruster. A Hall thruster operated with Xenon as the propellant has high efficiency (≥50%) and a specific impulse in the range where most missions optimize (I_{sp}=1200 to 2000 sec). A cross-sectional schematic of a Hall thruster is shown in Figure 2. The propellant is introduced through a special distributor into a dielectric annular discharge chamber where the pressure is typically 10^{-4} Torr. The propellant distributor often functions as the discharge anode, receiving electrons that originate in a cathode which is external to the discharge chamber. The electrons enter the discharge chamber through an imposed radial magnetic field which traps the electrons and forces them to execute $\overline{E}x\overline{B}$ drift. This drift (a consequence of the Hall effect, hence the thruster's name) can be viewed as an azimunthal current (J_θ) that closes upon itself and can be 100 times larger than the axial current (J_z). The ratio of J_θ/J_z can be shown to be approximately equal to the Hall parameter (β). The high J_θ current increases the probability of impact ionization of the propellant and creates the strong axial electric field (E_z) that accelerates the propellant ions outward producing thrust. To function well, the ion-neutral mean free path must be large relative to the thruster size and the plasma can be viewed as collisionless.

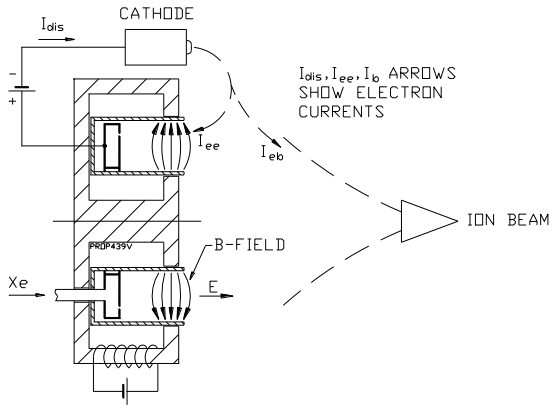

Figure 2 **Cross-sectional schematic of a typical Hall thruster with closed electron drift**

2.0 Phase I Results

To further the goals of the MABHET project, we have run a Hall thruster on a gas mixture that simulates the Mars atmosphere; analyzed thruster operation with carbon dioxide (ease of physics versus mixture) and looked at inlet design in the free molecular flow regime. The gas mixture simulating Mars was composed of 95.7% CO2, 2.7% N2, and 1.6% Ar.

Figure 3 shows a 1500 Watt Hall thruster running on simulated Mars mixture in a vacuum tank at Busek. The thruster is a standard xenon Hall thruster which has not been modified in any way. The characteristic "jet" can be seen, though somewhat more faint than with xenon, showing that the thruster is in typical high performance operation.

Figure 3 Hall thruster running on CO2 in Busek facility

As will be shown later, the important number for the thruster is the thrust to power ratio. This is because the thruster must overcome drag with some margin for maneuvering/reserve, so for a given power it is only the thrust that matters. Since it is using in situ propellant, the specific impulse is effectively infinite. Figure 4 and Figure 5 display the thrust to power ratio versus voltage at fixed flow and versus flow at fixed voltage respectively. As will be delineated later in the discussion of Hall thruster performance, typically the thrust to power will increase as the voltage is lowered to a point below which it then decreases. A maximum is also reached as the flow is lowered, although this phenomenon is not as well understood. The actual thrust increases with voltage [Figure 6], but the power increases quicker as both the voltage and the current are increasing. Since increased thrust would lead to a more compact thruster, the previous statement about the thrust to power being the important number is true only as long as the inlet is larger than the Hall thruster. In general, the performance evaluation says that the inlet is significantly larger than the Hall thruster, so the previous statement remains valid.

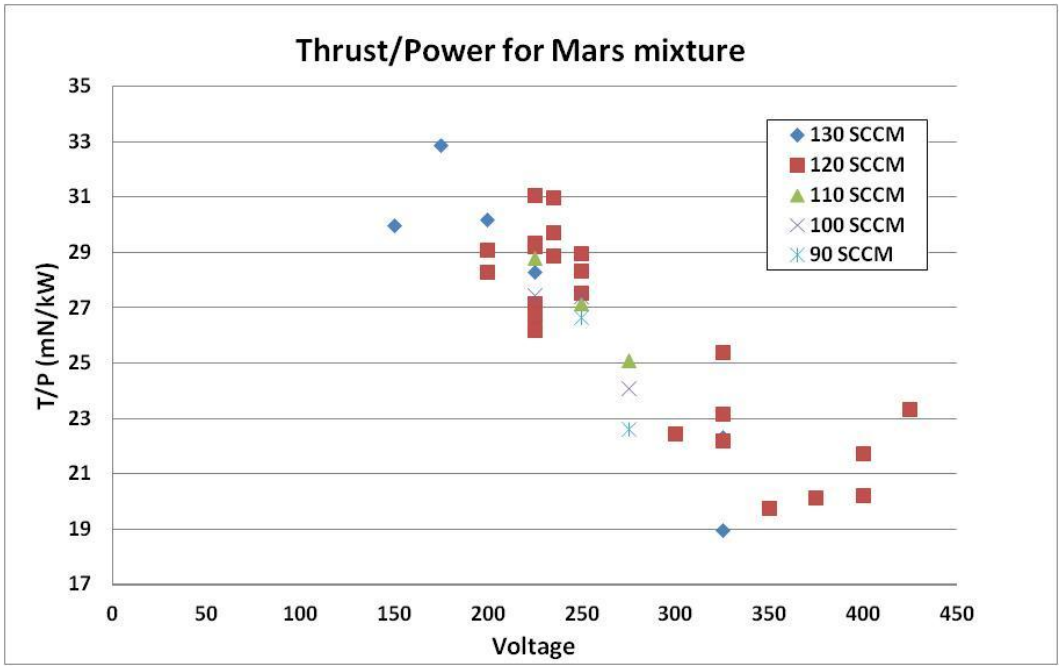

Figure 4 Thrust to power versus anode voltage for Hall thruster running on Mars mixture

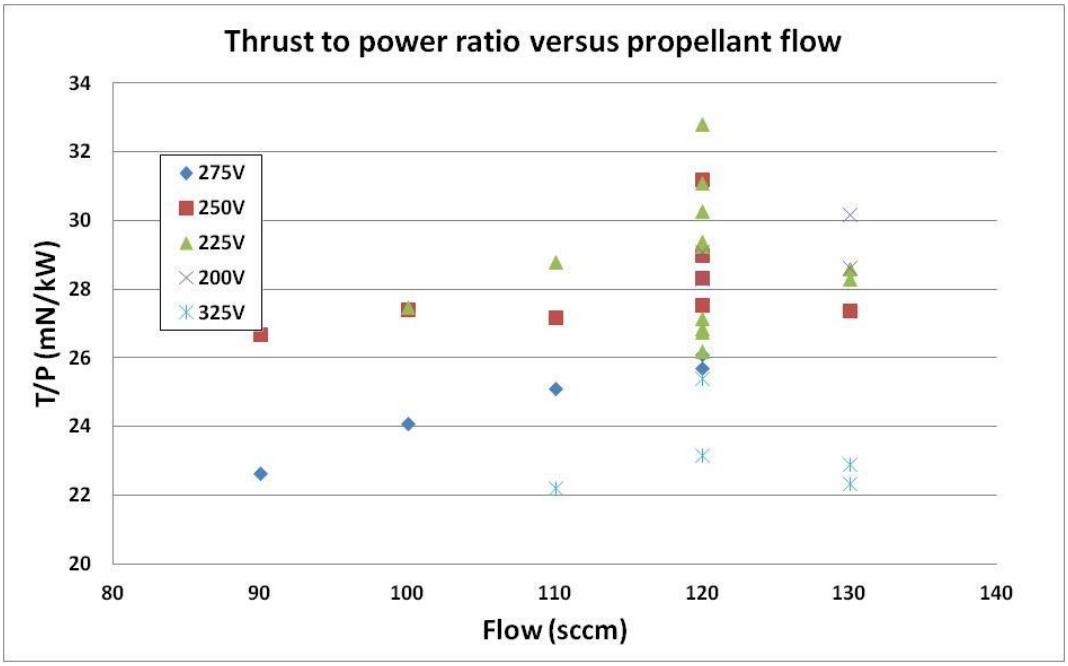

Figure 5 Thrust to power versus gas flow at various anode voltages for a Hall thruster running on Mars mixture

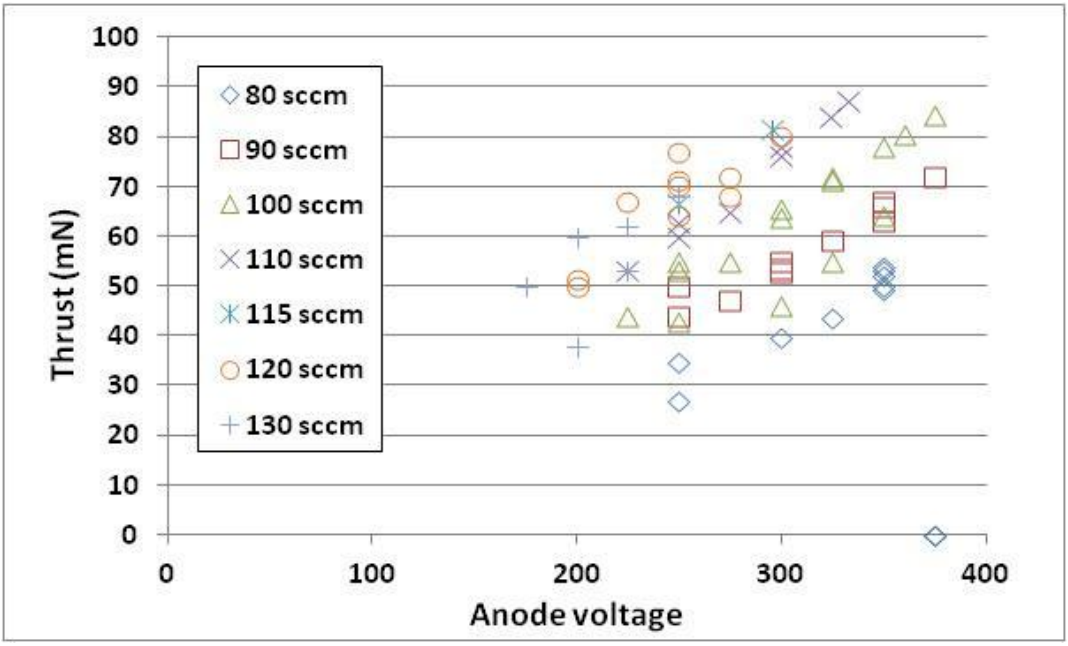

Figure 6 Thrust versus anode voltage for Hall thruster running on Mars mixture

One additional concern was whether the CO_2 oxidized the anode or if carbon soot precipitated out of the discharge. The thruster was operated for over 10 hrs without any evidence of oxidation or soot. Though more hours need to be logged before a claim of no concern, these results are very encouraging. Next we will show that CO_2 likely remains whole.

2.1 Hall Thruster Model for CO_2

Hall thrusters are usually designed to operate with xenon. The two main differences running on carbon dioxide mixture are that the particle mass is lower and the energy cost per ion accelerated is higher as compared to xenon, both of which decrease the thruster efficiency. The cost per ion will be higher for CO_2 than for xenon (or other noble gases) because of the extra energy cost per ion due to vibrational molecular states, rotational states, and dissociation. In spite of the efficiency being lower, our calculations show that the efficiency is sufficient to run a successful MABHET in the Martian atmosphere.

The ideal thrust to power is the ratio of the momentum carried per particle (mv) divided by the energy per particle ($\frac{1}{2}mv^2$), or $2/v$. To get the thrust to power, this is multiplied by the efficiency, which to a first approximation is just the energy of the particle divided by the sum of the energy per particle and the ion energy cost.

Figure 7 shows the calculated thrust to power for xenon and carbon dioxide, assuming an ion energy cost of 125 eV for Xe and 200 eV for CO_2. Figure 8 shows thrust to power calculations for CO_2 for three different ion energy costs in eV.

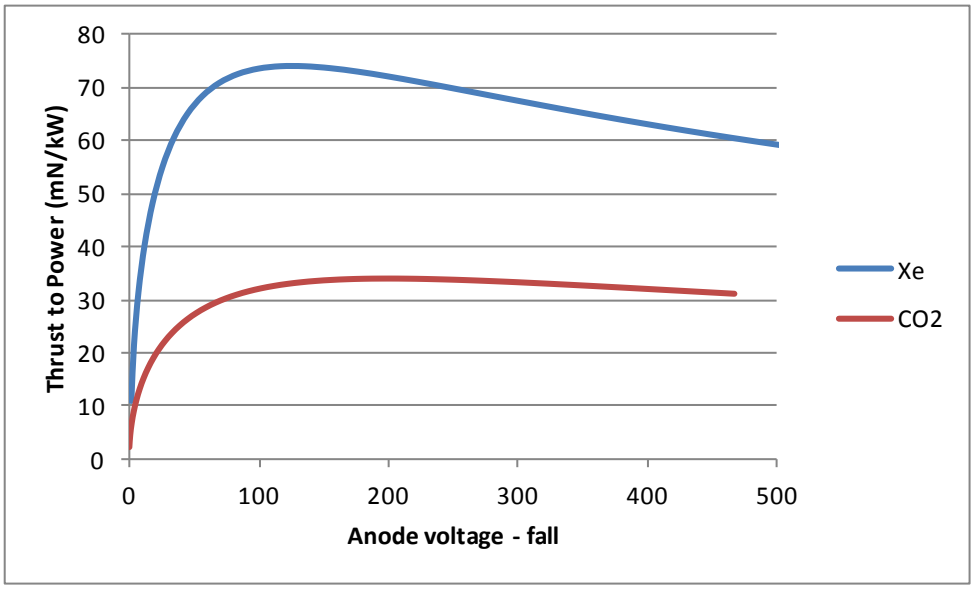

Figure 7 Calculated thrust to power versus voltage for Xe (125 eV ion energy cost) and CO_2 (200 ev ion energy cost)

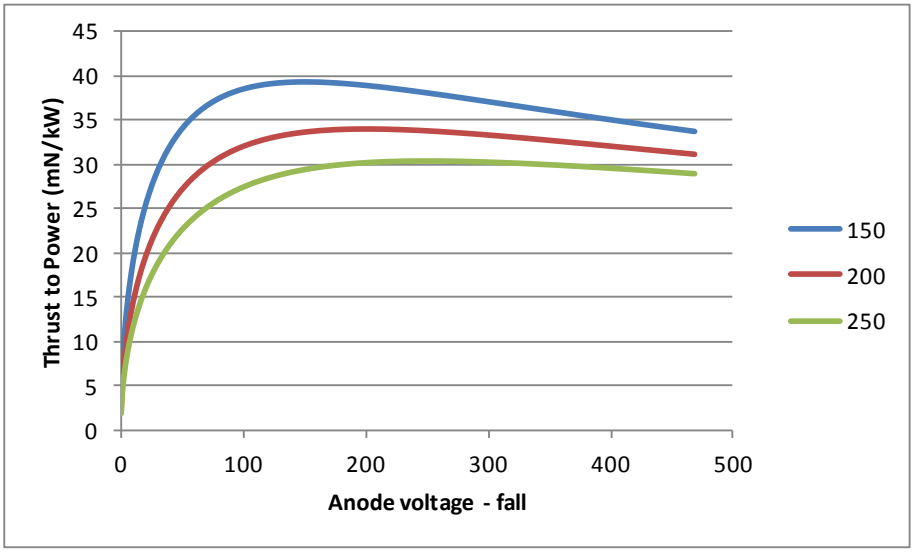

Figure 8 Calculated thrust to power for CO_2 at 3 different values of ion energy cost

The energy ion cost in general is shown below in equation 1. For our pressures, the elastic collision term is fairly small, so the second term in the sum can be neglected. The ion energy cost is thus the ionization energy plus a contribution due to the excited states.

$$E_{loss} = E_{iz} + \sum_{k=1}^{N_{exc}} \frac{\nu_{exc,k}}{\nu_{iz}} E_{exc,k} + \frac{\nu_{elastic}}{\nu_{iz}} \left(\frac{3mT_e}{M} \right) \quad [1]$$

For noble gases such as xenon and electron temperatures on the order of tens of eV or less, only the first three excitation levels make a significant contribution. At the minimum point on the curve for xenon, at about 20 eV, the contributions are ~12 eV for ionization, 8 eV for the first excited state, 3 eV for the second excited state, and 1 eV for the third excited state, for a total of 24 eV. This total of about twice the ionization energy is typical for noble gases.

For carbon dioxide, there are more contributions. Just knowing the energy cost is higher for carbon dioxide gives us some useful info, however, as shown in the figures above. This explains why the peak thrust to power occurs above 200 volts on the anode, and the numbers are not too far off from the data either, at ~ 30 mN/kW. The calculation seems to fall a little less rapidly than the experimental data, and in a separate calculation, the specific impulse, especially at high voltage, is lower for experiment than calculation. This may mean the propellant utilization is falling off faster than expected.

Another difference found with carbon dioxide compared to xenon is that sometimes it is harder to find a minimum in the current, i.e. the current decreases with increasing magnet until the thruster shuts off. A possible explanation is that the energy cost per ion decreases with increasing electron temperature out to a higher value. This is generally true for diatomic or higher gases. As the magnet increases, the electron temperature should increase as the potential steepens. Since there must be a balance of ionization rate versus loss rate, the plasma could go out before the minimum is reached. This is analogous to the situation in an RF-generated plasma where the electron temperature increases as the neutral pressure is lowered until finally the ionization can no longer keep up as the loss to the walls increases with temperature and the ionization curve flattens, so the plasma goes out.

The conclusion from this analysis is that the Hall thruster running on carbon dioxide mixture is performing about as might be expected, with a thrust to power ratio just over 30 mN/kW. It may be possible to improve this somewhat, but there is no obvious way forward. It may be worthwhile to spend some time on Hall thruster optimization with carbon dioxide, but there are greater returns elsewhere per unit effort, such as on the hyperthermal inlet and the drag along the surfaces.

2.2 Inlet Evaluation

To generate enough thrust to overcome the drag, an MABHET must collect a sizeable fraction of the gas it encounters and use that to fuel the thruster. The Hall thruster entrance is much smaller than the total frontal area of the satellite and the air must be taken in through a large inlet, compressed and passed through a much smaller aperture to the HET.

At the altitudes where an MABHET could operate the atmospheric density is so low that for a reasonably sized vehicle the incoming flow is collisionless. That is, it consists, at least initially, of individual molecules bouncing around in whatever chamber they enter. But if the passage to the HET is much smaller than the entrance to the collector, almost all such randomly-walking molecules will just reflect back out the entrance and the collection efficiency will be poor.

This situation can be improved by taking advantage of the fact that the incoming flow has high Mach number, i.e., it is well collimated. One can use a collection tube, a long cylinder aligned with the flow, as sketched in Figure 9. As illustrated, this creates a much higher density of trapped gas at the back of the tube, increasing the chance that a molecule will go out the exit to the thruster, not back out the entrance of the tube.

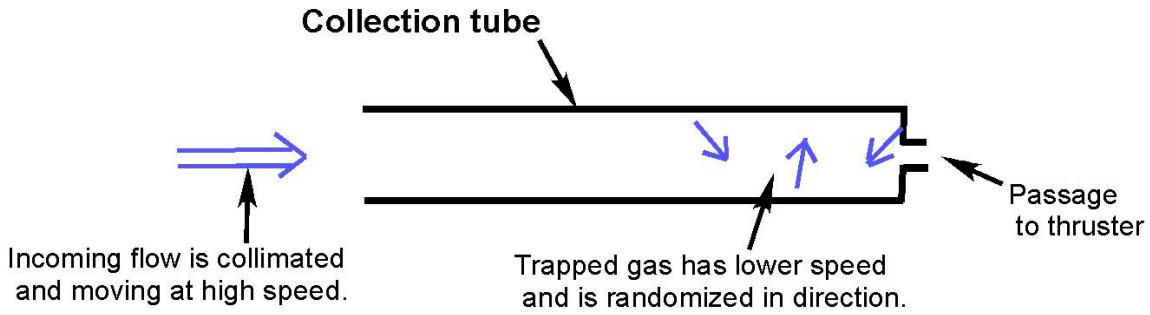

Figure 9 Conceptual diagram of inlet process

The density of the gas in the back of the tube can be a hundred times the density of the incoming flow, and mean free paths are reduced proportionately. This makes it possible for incoming molecules to collide with trapped molecules, pushing them toward the back to the tube. Indeed, one can get a cascade where a fast incoming molecule strikes a slow trapped molecule, and each of them then strikes other molecules. The effect is to push a considerable number of molecules in the desired direction, toward the passage to the thruster. Our study of this problem has convinced us that such "collisional pushing" is essential to good collection efficiency.

This is supported by studies of simplified collection tubes with a Direct Simulation Monte Carlo (DSMC) code.[5] The results of one such run are shown in Figure 10. That collector is a simple inlet cylinder, 60 cm in diameter, 3.7 m long, with an exit aperture 14 cm in diameter. Initial focus was on larger sized vehicle, thus the larger dimensions. We have simulated much smaller dimensions at appropriately increased density and found identical results. To determine the collection efficiency, a totally absorbing surface was placed right after the exit hole. In the output figure, the curved equidensity contours are evidence that the incoming gas is collisionally pushing the trapped gas toward the back of the tube, increasing the collection efficiency.

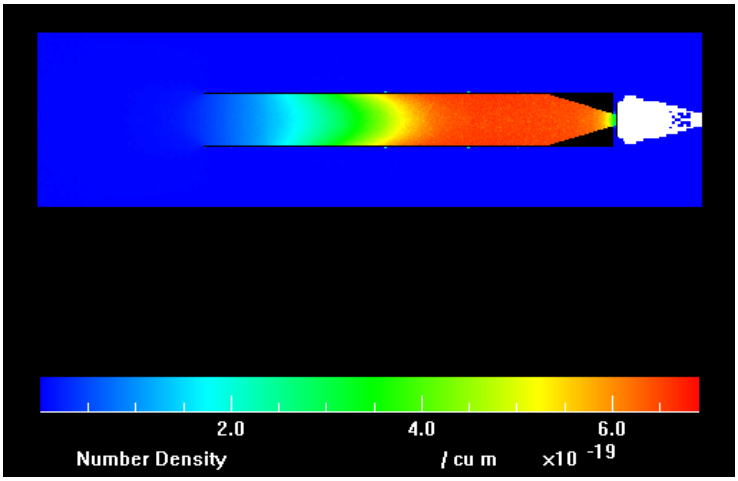

Figure 10 Density distribution predicted by the DSMC code for a collection tube 60 cm in diameter

What matters most is the ratio of the collisional mean-free-path to the tube dimensions, i.e. the product of the incident gas density times the tube diameter. Runs were made for a range of densities to determine this dependence. The results are shown in Figure 11. We find that good efficiencies are achievable if the density is high enough and the tube is large enough.

In these simulations, the entrance to the tube had an area almost twenty times the exit aperture to the thruster, yet the device collects almost forty percent of the incident gas, and that fraction is still going up as the density–diameter product increases.

The result makes sense. For an efficient cascade, one needs a collisional mean free path much less than the diameter of the tube. For a head-on collision that drives the struck molecule toward the back of the tube, one expects a cross-section of 10^{-19} m^2 or less. To make the mean free path a tenth of the tube diameter that means one needs a density-diameter product at the back of the tube of 10^{20} m^{-2}. Allowing for a 100× compression of the gas in the tube, one then needs at least 10^{18} m^{-2} based on the density of the incoming gas, which is what the simulations show.

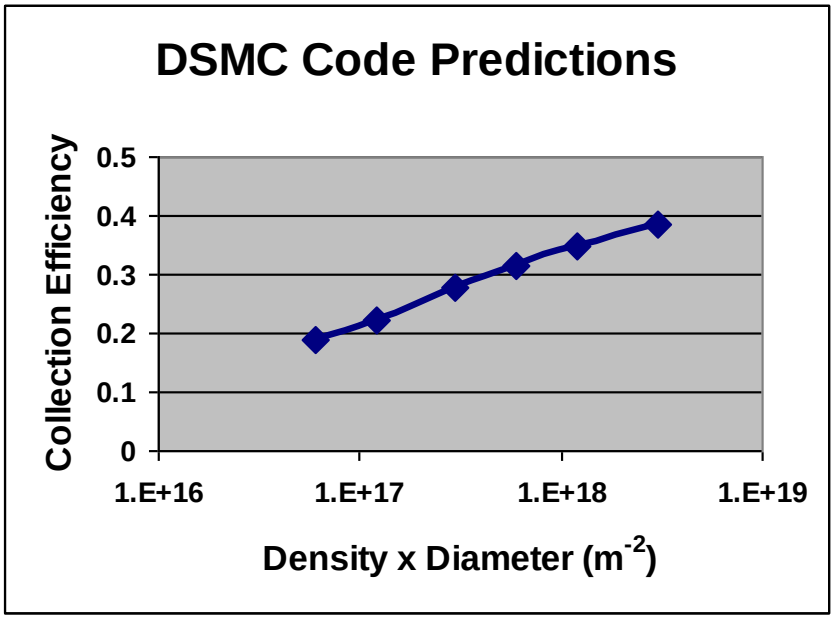

Figure 11 Collection efficiency predicted by the DSMC code. The density used here is the density of the incoming gas

2.3 Concept Evaluation in Realistic Application

Using realistic values for thruster performance, overall performance evaluations have been updated. For these calculations we assume an inlet frontal area of $0.15m^2$. Figure 12 shows the thrust required to counteract drag versus spacecraft altitude for various drag coefficients, Figure 13 does the same for power given the experimentally derived thrust to power, and Figure 14 for the collection coefficient. The important takeaway from this is that at a drag coefficient of 2.2 the requirements fall in the existing range of thruster performance and nearly the designed hyperthermal inlet, whereas the mission becomes more difficult as the drag coefficient increases. Also note that these calculations are for frontal drag area of double the inlet cross section of $0.15m^2$, or $0.30m^2$, for solar array structure.

Spacecraft orbiting Mars have a variety of possible orbits for various missions, which orbit can have a significant impact on the power available to the spacecraft. A sun-synchronous orbit could be designed to always face the sun so the spacecraft would have full power at all times and the solar panels could be aligned parallel to the flow to minimize the effective frontal area, in fact making it equal to the inlet area. This is the ideal situation for the MABHET. An example of a mission that could use such an orbit is sampling the atmosphere, a mission the

MABHET is ideally suited for, as it provides a means to measure the atmosphere at lower altitudes for unlimited times, which other spacecraft not using the in situ Mars atmosphere cannot do.

For other orbits, the situation is somewhat more difficult, since the solar panels may not be facing the sun or parts of the orbit may be shadowed. Since drag at low particle incidence angles is potentially specular, the best solution for these orbits is to extend the area of the solar panels to increase the power available. If the reflection is specular, there is almost no drag on the sides of the spacecraft, so such extension of size will not appreciably add to the power required. Decades of laboratory experience indicate that particle reflection is far more apt to be specular when the incidence angles are small, as would be true on the sides. With the extra power we could then accept the cosine loss of power if the panels are not facing the sun, and add batteries for the shadow period, thus still holding the spacecraft frontal area to the inlet area. Future efforts will address through both experiment and simulation ways to ensure low drag on the sides.

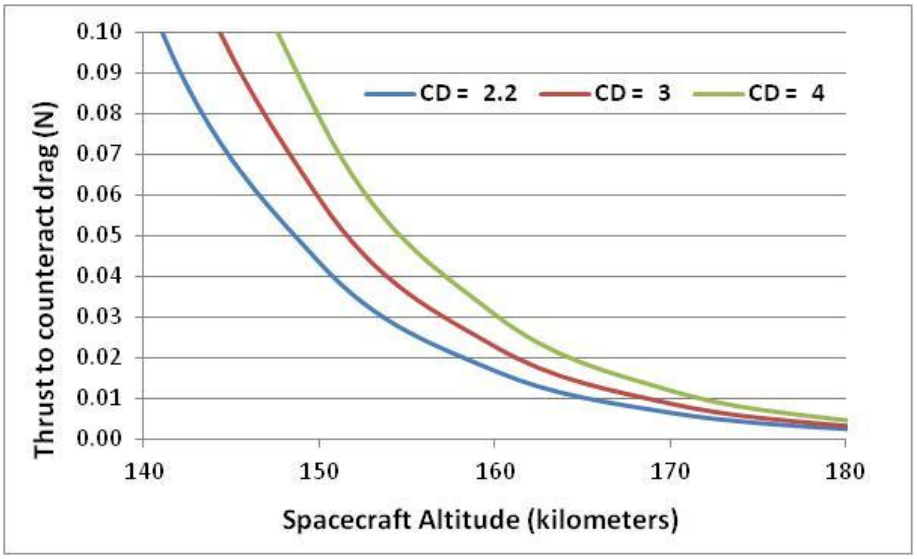

Figure 12 Thrust to counteract drag assuming different drag coefficients

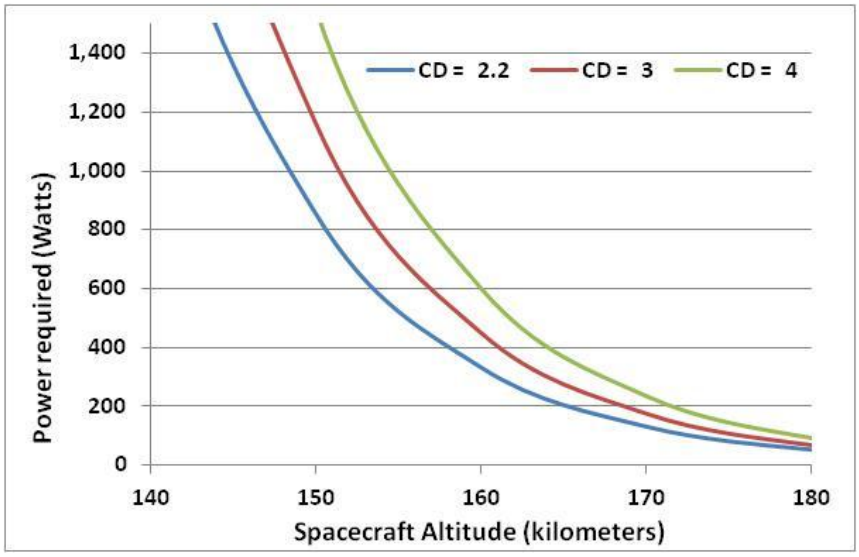

Figure 13 Power required to overcome drag at different drag coefficients

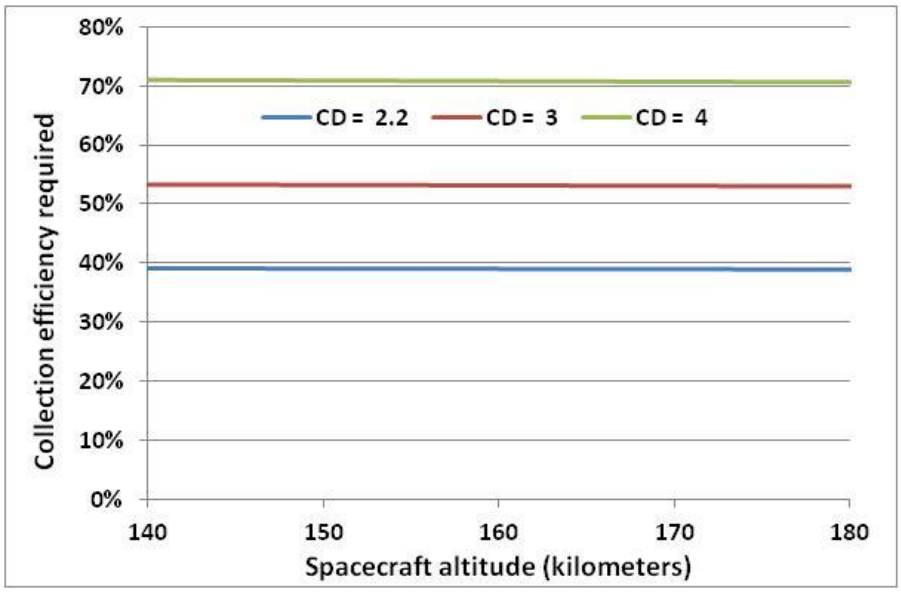

Figure 14 Collection efficiency required to overcome drag for different drag coefficients

2.3.1 Thermal Issues

There are two potential thermal issues. One is the usual necessary heat rejection from the power supply and the thruster itself. The other is due to the fact that the spacecraft is flying fairly low, so we should look at the heating due to friction.

To look at the latter issue first, it can be seen qualitatively that this should not be much of an issue if the MABHET is working as desired, i.e maintaining its altitude within the atmosphere. If the collection fraction is reasonably high, e.g. 25%, the power present in the exhaust will be higher than that in the incoming gas. A typical exhaust velocity for the Hall thruster is 15 km/sec, compared to less than 4 km/sec relative velocity of particles entering the inlet, so the particle energy in the exhaust is almost 15 times, leading to power in the exhaust being between 3 and 4 times that of the incoming gas. So, heat rejection is at worst about

comparable to that of the thruster and is not a big issue. To be more quantitative, Figure 15 shows the thermal power incident on the nominal spacecraft (frontal area 2 x 0.15m^2), showing that the incident thermal power is indeed expected to be low and in fact is much lower than the thermal power lost in the thruster.

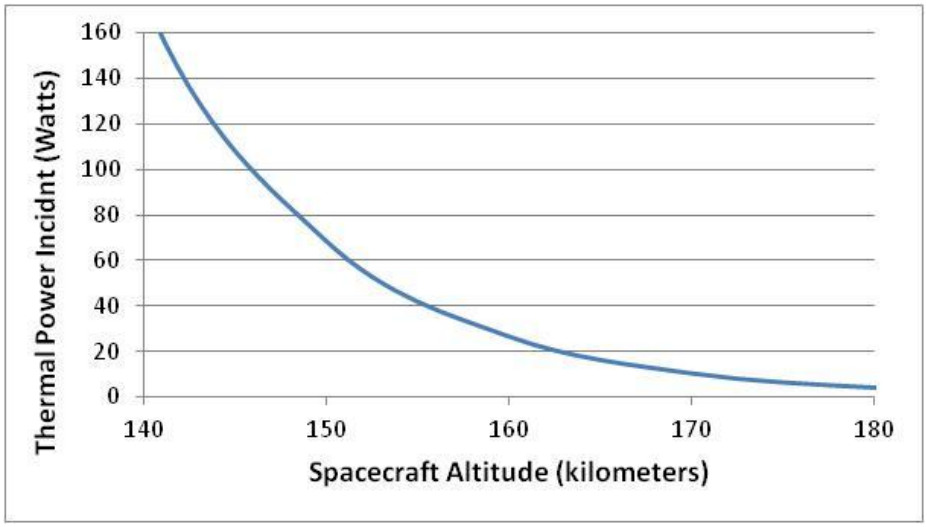

Figure 15 Thermal power of particles incident on the spacecraft versus altitude

As for the heat rejection capabilities of the spacecraft, Figure 16, shows the power radiated from a surface equal to the solar cell surface area for the nominal spacecraft, which could be the underside of the spacecraft. If the radiating surface is staring into space, the heat rejection capability is more than adequate, but even if it is staring at Mars it should be adequate, especially taking into account that Mars is colder than Earth.

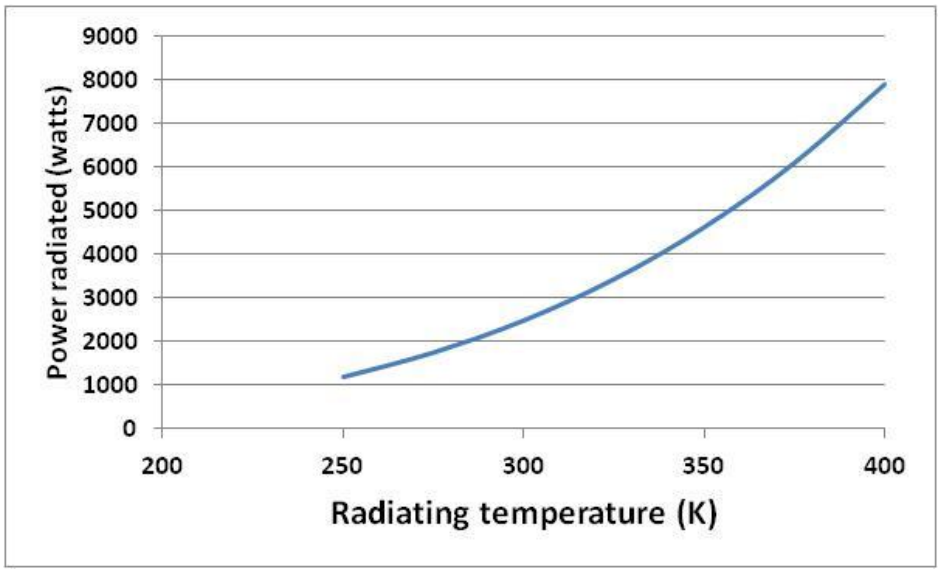

Figure 16 Thermal power radiated versus temperature of radiating surface

2.3.2 Accommodation

Accommodation is important to the MABHET in two ways, the overall drag coefficient and the efficiency of the collector, both of which will be improved if there is an element of specular particle scattering in addition to diffuse scattering. Drag is low if reflection is specular

and the angle of incidence is low, since the incoming particles in this case are little changed in either momentum or energy by the collision. The inlet works better, because it is easier to direct particles farther into the inlet rather than coming back out the front, which occurs with diffuse reflection.

For the drag coefficient, what is in particular important are the relatively long sides of the spacecraft which are necessary for solar cells to provide power for the thruster and for the inlet to have a high collection efficiency. For a relatively short spacecraft, with an aspect ratio near one, the drag coefficient would be expected to be about 2.2 with fully diffuse scattering. However, as the aspect ratio increases, the drag coefficient increases as particles move due to thermal motion and strike the sides from lateral positions beyond the frontal area of the spacecraft. If the reflections were completely specular, such collisions would provide little drag, but fully diffuse, accommodated scattering will provide a drag equal to the full momentum of the particle, since the particles would come off at the thermal temperature of the spacecraft surface, much less than the orbital velocity which the particles come in at. In the accommodated case, the effective frontal area is increased. For a circular cross section, the increase in radius is equal to the ratio of the thermal particle velocity at that altitude to the orbital velocity times the length of the spacecraft. The accommodation coefficients for the MABHET spacecraft can vary from those of satellites around Earth both because the composition of the atmosphere is different and the orbital velocity is different. The Mars atmosphere is mostly carbon dioxide and the circular orbital velocity is ~3.5 km/sec. Quite a body of work exists, both experimental and simulations, of spacecraft interaction with the atmosphere because of aerobraking, e.g. Mars Global Surveyor. Aerobraking near Venus, e.g. Magellan, is also relevant because the Venusian atmosphere is also largely carbon dioxide. Several features from this data set suggest that the MABHET may in fact work better than a similar craft in Earth orbit.

First some background on accommodation coefficients in general. In the region in which the MABHET is to operate, the flow is in general in the free molecular regime, i.e. the particles interact with surfaces much more than with each other. There are three types of particle collisions with surfaces, a specular collision in which the particle reflects like a light beam with equal angles of incidence and reflection and loses very little energy, a diffuse reflection in which the particle reflects into all directions, but does not equilibrate to the surface temperature, and a fully accommodated diffuse reflection in which the particles come off in all directions at the temperature of the surface. Since the orbital velocity corresponds to a temperature much higher than surface temperatures, in the latter case the particles essentially give up all their energy and momentum to the spacecraft. In low earth orbit, the last is often the case, which has been traced to an oxygen layer which forms on the surface due to the high reactivity of atomic oxygen, a significant component of the atmosphere at this level. This full accommodation takes place partly to the absorption/desorption which takes place on the surface, serving to equilibrate the temperature to the surface, and also to collisions with the oxygen layer itself. Since the oxygen atoms are weakly bound and are similar in mass to the incoming particles, they will tend to absorb both energy and momentum. Figure 17 displays the theory for the specular and diffuse scattering while Figure 18 shows a more likely scattering named CLL, which is a combination of the two.

The evidence from Magellan[6] and Mars Global Surveyor[7] indicate that the situation in Mars orbit may be better. Magellan showed an estimated energy accommodation coefficient of 0.63 for the solar panels, which is a fairly large specular component. It also showed a difference in materials of accommodation coefficient of 0.2 or more, which is also fairly substantial and

shows the importance of picking the right materials to reduce drag. If the 0.63 accommodation number is the one relevant for our case, that would result in a relatively low drag contribution from the sides and allow a large amount of power for a spacecraft with a low effective frontal area.

Another interesting item form the Mars Global Surveyor is that it appeared that density built up in front of surfaces. This is exactly the mechanism that we have proposed to use for the inlet to increase the density in front of the Hall thruster and also to collisionally prevent particles from leaving out the front.

In general, specular reflection is aided by small angles, clean smooth surfaces, high velocities, and a molecular mass in the surface particle which is heavier than the mass of the incoming particles.

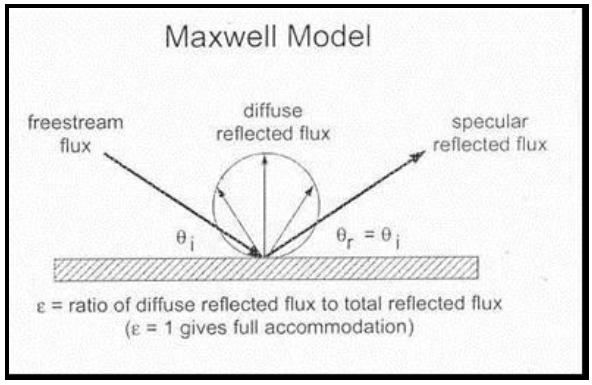

Figure 17 Schematic Representing Specular and Diffuse Reflection

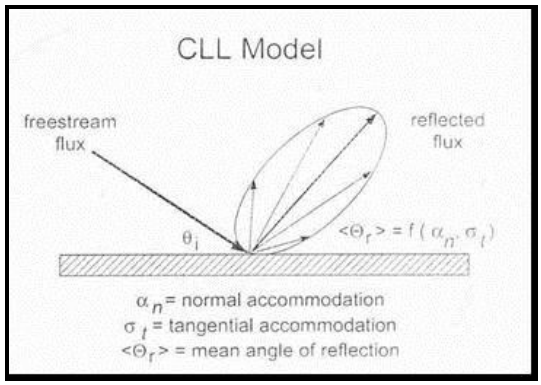

Figure 18 Schematic Representing the CCL Reflection Model

2.4 Testing and Characterization of Radio Frequency Neutralizer on Carbon Dioxide

Operate existing RF cathode and measure performance with gasses that simulate Mars atmosphere. The gasses of choice will include 100% CO2 and one or two mixtures consisting of CO2 and either argon or top 3-5 gasses the Martian atmosphere is composed of. Measurements will include emission current as a function of gas mix, flow rate, and input power/reflected power.

AVeeco SPECTOR ion beam deposition chamber was used to conduct all testing. This system contains two gridded RF (radio frequency) sources, as well as two RF neutralizers (RFN). The primary function of these neutralizers is to produce and emit electrons, minimizing space charging effects produced by ion beams. These were the commercially available neutralizers used for this testing.

Figure 19 shows a cross section of the neutralizer's construction. In this configuration the RF coil inputs energy to ionize the gas, creating and sustaining a plasma discharge. The RFN operates at powers ranging from 0 to 100 W, at an excitation frequency of 13.56 MHz. A keeper is biased to extract electrons from the plasma, creating the neutralizing effect for the ion beam. Finally, the collector attracts excess ions to compensate for the extraction of electrons. These neutralizers typically emit 100 – 900 mA of current when operating on 5 sccm Ar, and can reach temperatures of approximately 350 °C.

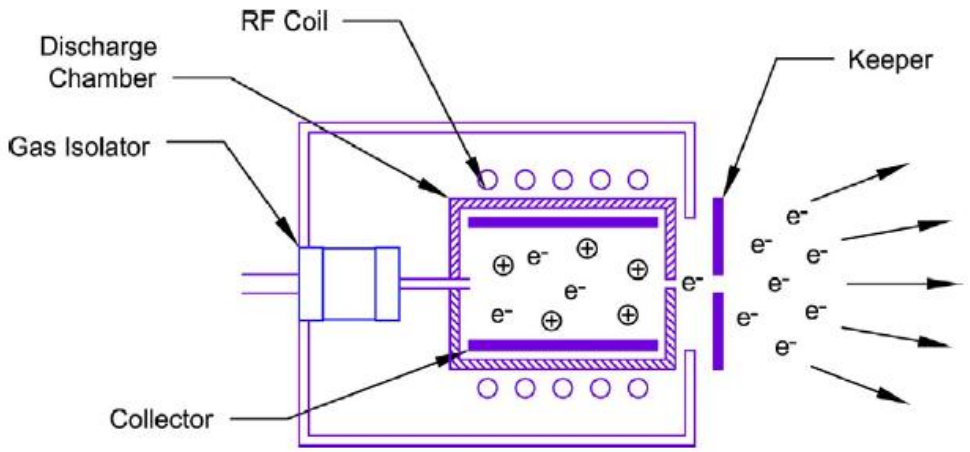

Figure 19 Cross section of the RFN (from Plasma Process Group, Inc. - Radio Frequency Neutralizer Manual)

Like any RF equipment, the neutralizer is reliant on a matching network to tune system to maximize forward power and minimize the reflected power. The power supply used was the original RF 2070 (Ion Tech, Inc.) unit that was installed on the SPECTOR system. This supply contained the RF generator as well as both DC supplies responsible for biasing the keeper and collector. The matching network and electrical connections are shown in Figure 20. The standard SPECTOR software package was used to command the RF 2070. An associated matching network contained two variable capacitors allow network tuning. Any changes to the collector shape or material would require a retuning of the network.

The start cycle of the RFN was completely automated. During this cycle, forward power would ramp and hold at 100 W for a few seconds while biases were placed on the keeper and collector. Power was then decreased and the system was monitored emission current. This would continue for 10 cycles if no emission current was detected before triggering an alarm. The start cycle could then be reinitiated. If sufficient current was detected, the RFN power would be set to 65 W at an emission current of 500 mA for a 5 minute warm up. After warm up the neutralizer would go to operating conditions set by the user.

Shunt resistors were installed in the power lines going to the keeper and collector. Voltages on either side of the resistor were measured and recorded using an Agilent 34970A Data Acquisition unit and an Agilent 34901A multiplexer (Figure 21). Line currents were calculated using the measured voltages and the known resistance of the shunt. Data acquisition calibration was performed using a separate stand alone power supply.

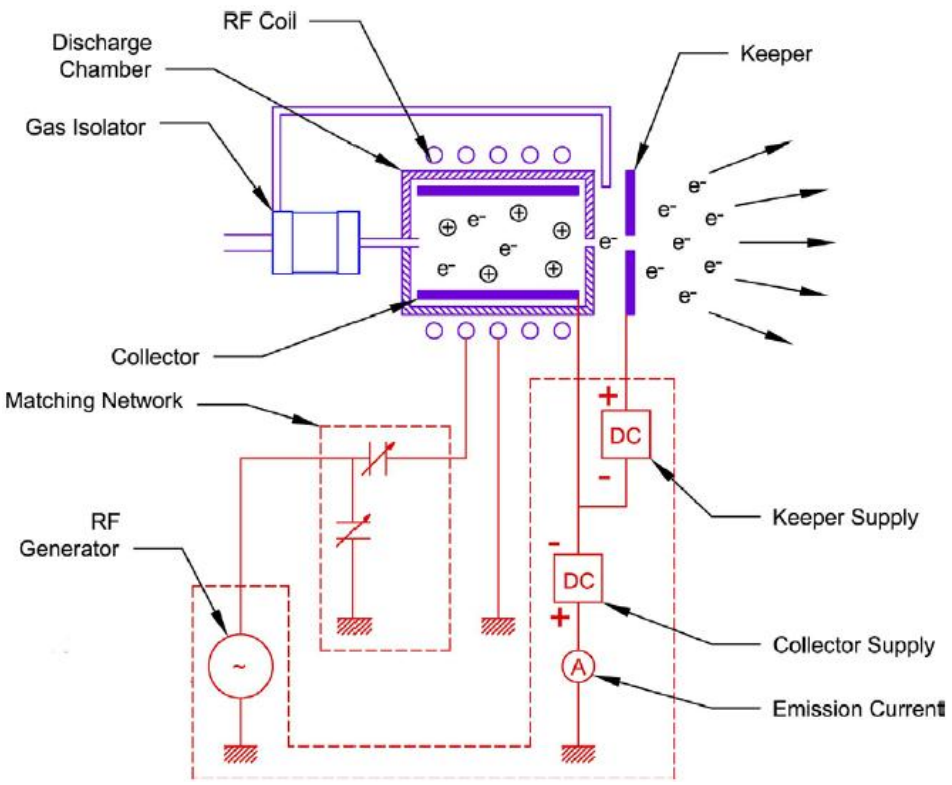

Figure 20 RFN electrical diagram (from Plasma Process Group, Inc. - Radio Frequency Neutralizer Manual)

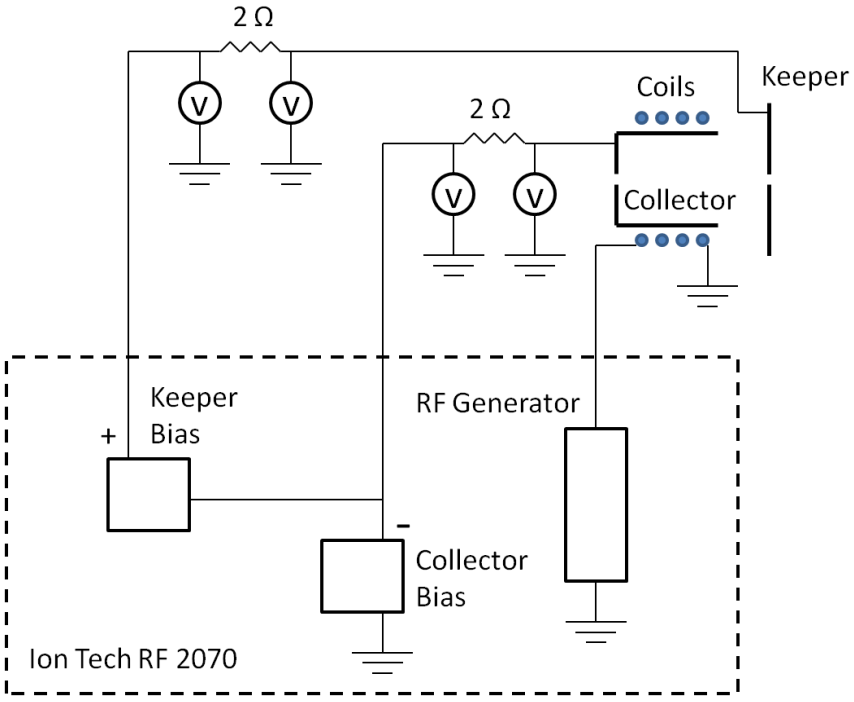

Figure 21 Electrical schematic including monitors

One of the key components dictating the performance of the neutralizer is the collector. Traditionally, this piece is constructed from nickel, limiting operation to the use of noble gasses since nickel is prone to oxidation. Oxidation can hinder RFN performance to the point where the neutralizer can no longer start or operate at the necessary emission currents. This was a concern when operation on CO2 was considered, due to the propensity for dissociated oxygen to attack the material. For this reason copper, titanium, and silver collectors were constructed. To minimize the impact of collector replacement on RF network matching, the original collector dimensions were mimicked as closely as possible. After each new collector was installed, the system tuning was optimized to the best possible running conditions (as measured by setting the forward power to 100 W during the start sequence, and minimizing the reflected power during operation).

Standard Nickel Collector

- Argon – Started easily, stable operation (operational data provided at the end of the report)
- CO2 – Could not start. Tried flow rates between 1-10 sccm CO2.

Copper Collector

- Argon – Started easily, stable operation (operational data provided at the end of the report)
- 98% Argon/ 2% Oxygen – Could not start
- CO2 – Could not start. Tried flow rates between 1-10 sccm CO2.

Titanium Collector

- Argon – Started, could not maintain a stable discharge. Tried flow rates between 1-20 sccm Ar.
- CO2 – Could not start. The power supply would indicate a discharge had begun but there was no emission current. Tried flow rates between 1-10 sccm CO2.

Modified Titanium Collector

- Argon – Started easily, stable operation (full data set not collected since focus was on starting with CO2)
- CO2 – Could not start. Tried flow rates between 1-10 sccm CO2. Additionally, attempted to raise the chamber pressure from 10^{-5} Torr up to 2 Torr over the course of 45 min while trying to start the RFN.

Silver Collector

- Argon – Could not start. Tried flow rates between 1-20 sccm Ar.
- CO2 – Could not start. Tried flow rates between 1-10 sccm CO2.

The existing equipment available for testing is not capable of sustaining a stable plasma discharge suitable for neutralization applications. No improvements could be observed despite attempted modifications to collector shape and material. Some of the possible reasons could be:

- Pressure/flow rates were too low – Most experiments using RF to generate CO2 plasmas are performed at 15-300 mTorr.
- Not enough power – It is possible that more than 100 W of power is necessary to start or maintain a stable discharge.
- Electric field not large enough – requires redesigning the matching network/coil combination and likely changing the RF frequency.

The values given in the following charts are approximate averages and do not give any indication for the stability of the discharge. Conditions that were particularly stable have been highlighted. Data marked with xxx indicates the condition was not stable enough to be read.

Argon with nickel collector

Gas Flow: 2 sccm Pressure: 5.7*10^-5 Torr

Emission Current	Forward P	Reflected P	Collector Voltage	Collector Current	Keeper Voltage	Keeper Current	Time Stamp
200	20	0	-104	250	-61	50	5:38
200	40	0	-65	xxx	-25	xxx	5:40
200	60	2	-70	xxx	-30	xxx	5:42
200	80	4	-80	xxx	-42	xxx	5:44
400	20	xxx	xxx	xxx	xxx	xxx	5:46
400	40	0	-100	xxx	-62	xxx	5:55
400	60	2	-102	xxx	-63	xxx	5:57
400	80	4	-102	400	-63	180	5:59
600	20	xxx	xxx	xxx	xxx	xxx	6:13
600	40	2	-107	230	-65	80	6:09
600	60	2	-104	350	-64	130	6:05
600	80	4	-102	421	-63	175	6:01
800	20	xxx	xxx	xxx	xxx	xxx	xxx
800	40	2	-107	240	-65	80	6:11
800	60	2	-104	340	-64	125	6:07
800	80	4	-102	410	-63	170	6:03

Argon with nickel collector

Gas Flow: 4 sccm Pressure: 7.0*10^-5 Torr

Emission Current	Forward P	Reflected P	Collector Voltage	Collector Current	Keeper Voltage	Keeper Current	Time Stamp
200	20	0	-41	350	-0.5	80	6:26
200	40	0	-25	510	8	300	6:28
200	60	2	-28	475	6	400	6:30
200	80	5	-31	300	5	800	6:43
400	20	2	-99	300	-48	0	6:45
400	40	0	-32	700	1	300	6:47
400	60	4	-32	700	0	200	6:49
400	80	6	-41	xxx	-8	xxx	6:58
600	20	2	-99	300	-50	0	7:00
600	40	1	-44	xxx	-7	200	7:04
600	60	3	-34	900	-6	400	7:06
600	80	6	-51	xxx	-19	xxx	7:08
800	20	1	-99	300	-50	0	7:10
800	40	1	-87	800	-49	50	7:12
800	60	3	-43	1100	-15	400	7:14
800	80	6	-55	1000	-24	600	7:16

Argon with nickel collector

Gas Flow: 6 sccm Pressure: 8.4*10^-5 Torr

Emission Current	Forward P	Reflected P	Collector Voltage	Collector Current	Keeper Voltage	Keeper Current	Time Stamp
200	20	1	-41	350	-1.5	100	7:20
200	40	1	-25	500	5	300	7:22
200	60	3	-26	510	5	360	7:24
200	80	6	-26	500	5	525	7:26
400	20	1	-97	350	-37	0	7:28
400	40	1	-31	700	-2	300	7:30
400	60	3	-28	700	-1.5	300	7:32
400	80	6	-29	700	-2	400	7:34
600	20	1	-97	350	-37	0	7:36
600	40	1	-45	xxx	-10	xxx	7:38
600	60	3	-32	700	-8	600	7:40
600	80	6	-32	1000	-8	200	7:24:20
800	20	1	-97	325	-37	0	7:44
800	40	1	-88	825	-51	100	7:46
800	60	3	-52	1000	-25	750	7:48
800	80	6	-45	1250	-20	0	7:50

Argon with nickel collector

Gas Flow: 8 sccm Pressure: 9.7*10^-5 Torr

Emission Current	Forward P	Reflected P	Collector Voltage	Collector Current	Keeper Voltage	Keeper Current	Time Stamp
200	20	0	-41	350	-2	125	7:56
200	40	0	-25	500	5	300	7:58
200	60	2	-25	515	5	260	8:00
200	80	6	-25	515	5	300	8:02
400	20	1	-96	350	-37	0	8:04
400	40	1	-29	720	-1	320	8:06
400	60	4	-27	700	-1	290	8:08
400	80	7	-27	710	-1	275	8:10
600	20	0	-96	350	-37	0	8:12
600	40	0	-44	800	-8	200	8:14
600	60	4	-29	920	-4	300	8:16
600	80	7	-29	920	-4	290	8:18
800	20	1	-96	350	-37	0	8:20
800	40	1	-65	xxx	-20	xxx	8:22
800	60	3	-31	1150	-7	320	8:24
800	80	7	-29	1120	-7	310	8:26

Argon with copper collector

Gas Flow: 2 sccm Pressure: 5.8*10^-5 Torr

Emission Current	Forward P	Reflected P	Collector Voltage	Collector Current	Keeper Voltage	Keeper Current	Time Stamp
200	20	1	-63	xxx	-22	xxx	4:08
200	40	1	-57	xxx	-11	xxx	4:10
200	60	1	-75	xxx	-37	xxx	4:12
200	80	3	-73	xxx	-37	xxx	4:14
400	20	1	xxx	xxx	xxx	xxx	4:16:20
400	40	1	-79	xxx	-40	xxx	4:18
400	60	1	-95	xxx	-58	xxx	4:20
400	80	3	-100	xxx	-63	xxx	4:22
600	20	1	-103	260	-61	70	4:24
600	40	1	-74	xxx	-40	xxx	4:26
600	60	1	-102	xxx	-62	xxx	4:28
600	80	3	-101	470	-63	210	4:30
800	20	xxx	xxx	xxx	xxx	xxx	4:32
800	40	xxx	xxx	xxx	xxx	xxx	xxx
800	60	xxx	xxx	xxx	xxx	xxx	xxx
800	80	xxx	xxx	xxx	xxx	xxx	xxx

Argon with copper collector

Gas Flow: 4 sccm Pressure: 7.1*10^-5 Torr

Emission Current	Forward P	Reflected P	Collector Voltage	Collector Current	Keeper Voltage	Keeper Current	Time Stamp
200	20	0	-36	400	2	180	4:55
200	40	0	-26	510	6	340	4:57
200	60	2	-27	475	5	600	4:59
200	80	5	-31	300	-3	1300	5:01
400	20	0	-95	400	-41	0	5:03
400	40	0	-30	700	-1	300	5:05
400	60	3	-35	xxx	-6	xxx	5:07
400	80	6	-50	xxx	-22	xxx	5:09
600	20	1	-95	400	-42	0	5:11
600	40	1	-38	900	-4	300	5:13
600	60	3	-37	xxx	-10	xxx	5:16
600	80	6	-64	xxx	-34	xxx	5:18
800	20	0	-96	400	-42	0	5:20
800	40	0	-87	925	-51	120	5:22
800	60	2	-46	xxx	-21	xxx	5:24
800	80	6	-72	xxx	-42	xxx	5:26

Argon with copper collector

Gas Flow: 6 sccm Pressure: 8.4*10^-5 Torr

Emission Current	Forward P	Reflected P	Collector Voltage	Collector Current	Keeper Voltage	Keeper Current	Time Stamp
200	20	0	-37	380	0.5	175	5:31
200	40	0	-25	520	5	300	5:33
200	60	2	-25	510	6	270	5:35
200	80	5	-25	510	3	675	5:37
400	20	0	-95	xxx	-20	xxx	5:39
400	40	0	-29	700	-2	300	5:41
400	60	3	-28	720	0	300	5:43
400	80	6	-27	720	0.5	300	5:45
600	20	0	-95	400	-36	0	5:47
600	40	0	-35	xxx	-5	300	5:49
600	60	2	-28	920	-4	290	5:51
600	80	6	-28	920	-4	350	5:53
800	20	1	-95	400	-36	0	5:55
800	40	1	-77	xxx	-42	xxx	5:57
800	60	3	-35	xxx	-10	300	5:59
800	80	5	-32	1300	-9	0	6:01

Argon with copper collector

Gas Flow: 8 sccm Pressure: 9.7*10^-5 Torr

Emission Current	Forward P	Reflected P	Collector Voltage	Collector Current	Keeper Voltage	Keeper Current	Time Stamp
200	20	0	-38	400	0	175	6:08
200	40	0	-24	500	5	300	6:10
200	60	2	-24	520	5	290	6:12
200	80	6	-23	520	3	400	6:14
400	20	1	-74	500	-18	0	6:16
400	40	1	-28	700	-1	300	6:18
400	60	3	-26	700	-1	300	6:20
400	80	5	-26	700	-1	300	6:22
600	20	1	-94	400	-36	0	6:24
600	40	1	-40	900	-5	300	6:26
600	60	3	-27	920	-5	310	6:28
600	80	5	-27	920	-4	330	6:30
800	20	0	-95	400	-36	0	6:32
800	40	0	-50	800	-13	100	6:34
800	60	2	-30	1100	-7	320	6:36
800	80	5	-28	1120	-7	310	6:38

3.0 Next Steps in Development

In our view, the path to MABHET realization includes 7 topics described below. The first, and most critical in our view, is Inlet Development, to investigate the development of an efficient atmospheric gas inlet that can ingest and initiate the collection of the Mars atmosphere gases. The second is Low Drag Design for Mars, potentially measuring gas-surface accommodation for conditions simulating Mars mission in our state-of-the-art facility. The third is Gas Compression to investigate gas compression both internal to the inlet and by mechanical means. The fourth is Thruster Optimization for operation on Mars atmosphere. The fifth area is the Cathode Neutralizer that operates on CO2. The sixth is the Overall Vehicle Design where all the systems and payload need to be determined and verified functionality. The seventh is Mission Infusion and could be the most critical because without a mission, no reason to pursue the concept. We discuss our thoughts on these topics next.

1.) Inlet Development

The more research completed on this concept, the more the inlet importance becomes relevant. To be more precise, it is the atmospheric gas collection efficiency of the inlet that drives the size of the inlet, which in turn drives the frontal cross section of the spacecraft, which drives the spacecraft drag. As was shown above, the gas surface interaction and particle reflection or accommodation is critical for gas collection. We suggest to further model the inlet with the Bird DSMC program AND perform experimental testing and confirmation. Busek is uniquely prepared to perform the experimental testing with our flux sources and test facilities. Directly related is the measurement of thermal accommodation coefficients for Mars gases with select materials and temperatures and that will be the focus of Task 2.

The inlet design was discussed above in the Phase I summary. It is based on the theory and modeling data that is based on the physics of rarefied hyperthermal flows and the HET propellant feed requirements. The rarefied gas – surface interaction and reflection depends greatly on the accommodation coefficient. Specular reflection will be much more favorable to gas collection versus diffuse, as the gas particles will naturally flow to the rear of the collection inlet. The HET requires a gas pressure at a few mTorr for efficient ionization, where as the ambient gas is typically a few to 100 microTorr. Since a pressure or density increase is required to operate the HET, we concluded that if, with a proper design, we could get the high velocity incident gas to collide with slower, trapped gas, two positive outcomes could be achieved: 1.) the gas would naturally compress and 2.) the volume in the collection tube would become collisional and a higher fraction could be collected and utilized.

The Knudsen number, ratio of particle mean free path over characteristic length, is >1 for the gas mean free path in orbit and the inlet diameter in our case. This indicates that continuum fluid mechanics laws break down and the problem requires statistical analysis. We will further our investigation by utilizing the DSMC program previously described. After the recent literature discovery that Magellan experience very specular nature on the solar arrays in Venus orbit (mainly CO2 atmosphere) we need to rerun the simulations with more specular accommodation.

The experimental focus will be to demonstrate a scaled inlet collection efficiency when subjected to a simulated Mars orbital flux. The key technology that allows us to perform this test is the high velocity source of highly directional CO2. Busek has developed two options for this source during previous programs. The first is an arcjet operating in vacuum to form a free jet expansion as shown in Figure 22. The CO2 could potentially oxidize the materials making up

the cathode and throat, though CO2 is fairly stable and could be run for short timeframes. The easier and less oxidation prone source is a Radio Frequency hot gas source we designate RFET based on our electrothermal thruster development. The RFET is shown in Figure 23. The plasma is generated via an inductively coupled discharge and thus, no electrodes are exposed to the plasma.

Figure 22 Busek arcjet operating in free jet mode

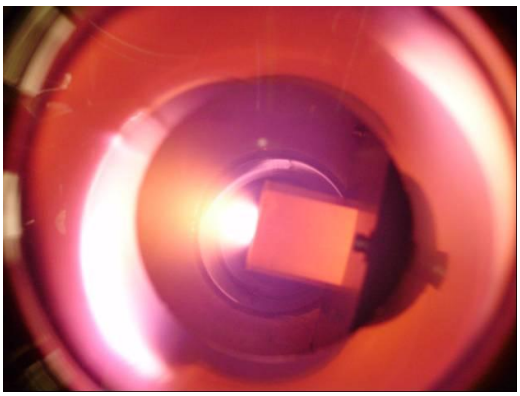

Figure 23 Busek REFT operating with nitrogen

The actual apparatus configuration will include the source, a modular inlet, and a turbomolecular pump. The first test will entail a blanked off inlet and we will measure the pressure build. We will then gradually open the back end of the inlet in specified setpoints, again measuring the pressure build. We can compare these results with the DSMC models. We will then calibrate the turbo-pump versus a known gas flow, or direct feed a known gas and measure pressure at the turbo head. We will then connect a test inlet to the turbo head and place in the CO2 hyperthermal beam. We will be able to estimate the fraction of gas incident on the inlet and compare to the pressure curve for actual gas collected.

2.) Low Drag Design for Mars

The actual drag coefficient of the proposed MABHET powered spacecraft is crucial to the success of this concept. We have based our analysis on a CD of around 3. That requires solar array efficiency of around 35% and inlet collection efficiency of around 35% just to counter drag. We know that short aspect ratios (as defined for airplane wings) or long spacecraft tend to have high CD due to the thermal gas particles hitting the long sides of the s/c. Our proposed vehicle fits this definition of a long s/c, so CD of 3 may indeed be the correct assumption. One counter to this argument is that data as mentioned above for Magellan and Mars Global Surveyor, where considerably lower CDs were measured.

We suggest to measure thermal accommodation coefficients with our unique micro-Newton torsion balance facility. We have demonstrated this capability on a previous program where we developed an Atomic Oxygen (AO) source to simulate LEO environment and utilized the torsion balance to measure drag on samples placed in this AO source beam. The torsion balance is shown in Figure 24 and a sketch of the concept of measuring the drag is shown in Figure 25. Busek successfully demonstrated this facility to measure thermal accommodation coefficient measurements as shown in Table 1.

Eliminating the requirement of producing 5eV AO by replacing with 2.9eV CO2 removes considerable difficulty from the process. We can utilize the source described in the previous task and skim the inner flux to obtain a uniform, well characterized beam. These tests will help

determine the accommodation coefficients of typical materials and help predict the CD. It will be very interesting to see if CO2 behaves close to AO or if it indeed, behaves drastically different as the data indicates. It will also help distinguish the AO layer that is believed to build up on surfaces in LEO versus gases such as CO2.

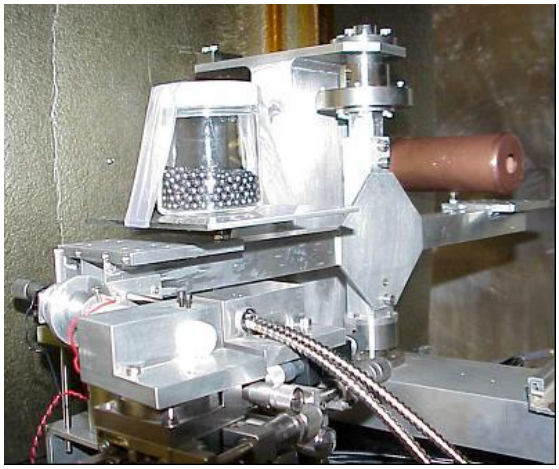

Figure 24 Busek micro-Newton torsion balance

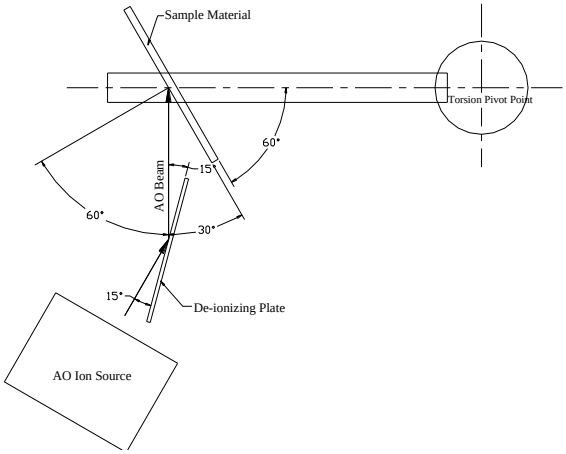

Figure 25 Concept sketch of drag measurements

Table 1 Example of measurements and calculations of accommodation coefficients for sample materials subjected to 5eV AO beam

material	target angle	$F_{parallel}$	$F_{45\ degrees}$	$F_{perp.}$	F_n 30	F_t	A	specular fraction	F_i	Accomm Coeff σ
grit SS	30	**17.8**	**12.6**	0.0	8.9	15.4	1.002478	0.0012	17.8	
glass	30	**19.4**	**15.2**	2.1	11.5	15.8	1.266116	0.1174	20.6	0.8826
Kapton	30	**13.7**	**9.6**	0.1	7.0	11.8	1.020936	0.0104	13.8	0.9896
SS	30	**12.4**	**16.0**	10.2	15.1	5.6	4.636411	0.6452	18.3	0.3548

3.) Mechanical Gas Compression

Our first choice would be not to include any mechanical compression if we can get the required performance statically. A mechanical compressor requires additional power and moving components that increase risk, especially on a spacecraft. Complete success in developing the inlet and low drag will make this task less critical. However, increased drag may require higher gas collection efficiency and we anticipate some optimization hurdles and thus suggest an additional mechanical compression of the collected gas as a risk reduction. The gas loads and pressure range of operation naturally leads one to a turbomolecular pump. Turbo-pumps are historically around 50% efficient at capturing the incident gas particles. The well collimated orbital flow should increase the collection efficiency fractionally, as a much greater percentage makes it past the first stage, versus the random thermal motion in a typical vacuum facility.

We suggest to investigate the capture efficiency of a standard, off the shelf turbo-molecular pump. This measurement is similar to the inlet testing, but will forgo the inlet and focus on the turbo pump as the gas collection entirely. We will investigate designs on the inlet

that may improve the collection efficiency. For instance, decreasing the first stage angle of attack would likely improve the collection efficiency for the well collimated flow. If we can engineer a simple change in house, we will install and compare the turbo pump performance. In parallel, we plan to contact the pump manufacturers such as Varian and Leybold and determine a practical means of designing and implementing an inlet for our application.

4.) Thruster Optimization

It was indicated above that we believe there is only minor optimization opportunity in the thruster design for operation with the Mars atmosphere. That being said, a little performance improvement can go a long way to realizing the MABHET success. Since drag is the major obstacle to adding more power (solar arrays), we wish to optimize thrust to power ratio while maintaining reasonable thruster efficiency. The analysis summarized above indicates that the energy losses expected with the CO2 mixture versus xenon appear to be right in line with the measured performance. It may be possible to optimize the thruster characteristic to operate in the high thrust to power mode more favorably. One possible way to achieve improved efficiency at the high thrust to power is to modify the discharge channel volume slightly. This is based on the higher thrust to power measured for lower flows in previous programs versus the higher efficiency at higher flows. The rational is that by decreasing the volume for a given mass flow, the particle density increases. We achieve higher efficiency at higher densities than at higher thrust to power densities. We will investigate this analytically and initiate an experimental investigation to determine if there are any improvements in thruster redesign for high thrust to power versus high efficiency.

5.) Cathode Research

All Hall effect thrusters require an electron source to initiate the discharge, supply free electrons to configure the electro-magnetic fields and neutralize the plasma in the plume to prevent spacecraft charging. The standard methods to supply this relatively high flux of electrons has been thermionic cathodes, almost exclusively xenon fed hollow cathodes. The hollow cathode contains a low work function material such as barium-oxide coated tantalum. At these high temperatures, greater than 1000°C, oxygen will attack the cathode and quickly leading to non-emission of electrons. It is not known a prior whether CO2 will poison the cathode , but it is believed that some fraction of CO2 will dissociate and the oxygen will greatly shorten the life of the cathode.

We suggest to operate an electron cyclotron resonance (ECR) microwave cathode with these same gases to determine the feasibility of using an ECR cathode in place of the hollow cathode. Busek has a small ECR cathode and has operated with gases that simulate a new high performance liquid monopropellant decomposition. This is important since a fraction of the gas is CO2 and O2. Figure 26 shows a picture of this ECR cathode and oxygen heavy gas.

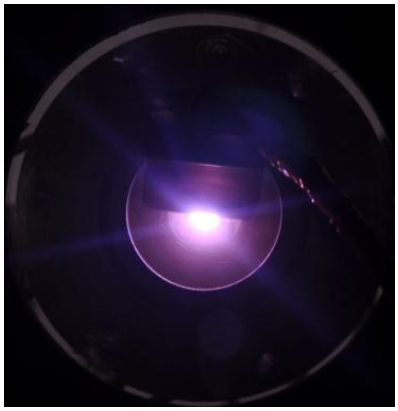

Figure 26 Busek's ECR cathode operating on gas mixture that contains CO2

6.) Vehicle Design

The spacecraft/vehicle design will be an evolving model over the years as more details of the propulsion system and its requirements are worked out. We believe that minimizing frontal area will be a key to our success and since we have ruled out any impact from lift, the "flying wing" concept does not seem appropriate at this point. The payload and thruster can trail the inlet without increasing the drag significantly, at least at very narrow angle of attack. The solar arrays can be minimized as their efficiency increases. The major issue we need to work out is the angle of attack versus location of the Sun and that really depends on the mission. One can envision missions where ~50% of the orbit, the panels can be positioned towards the Sun without increasing the drag profile. This requires panels sized 2x the power of the thruster and a battery system to store power for use in shadows or less optimum solar generation. Another option that should become available in 10-15 years is beamed power. In this scenario, an orbiting spacecraft at much higher orbits could beam power to the MABHET powered vehicle periodically. Microwave and laser power beaming technology is in development with promise of future capabilities. There are other, less practical or very futuristic, concepts that we will not include in our studies at this time.

The focus during Phase II will be on the inlet integration with a payload and thruster configuration, keeping in mind the low drag requirements. Busek has fabricated major subsystems for LEO spacecraft and can utilize that experience in this task. In addition, we will open dialogue with aerospace primes including Raytheon and ATK, both of which we have current programs with.

7.) Missions/Infusion

In order to infuse this technology into NASA missions, we need to find a scientific home where the MABHET performance enables the mission. Several example missions were mentioned in the introduction including low altitude orbital observation, measurements of crustal magnetism, atmospheric boundary layer composition, chemistry and dynamics and near-surface water. We plan to continue building support for our concept by attending Mars science conferences and meeting and pursuing NASA support as we go. We are attending the Concepts and Approaches for Mars Exploration Meeting this June in Houston, TX.

The primary advantage the MABHET brings to Mars missions is the ability to operate at lower altitudes for an indefinite time as compared to spacecraft which are not using the in situ Mars atmosphere for propulsion. Such a spacecraft can measure the atmosphere in a region for which there is no other direct access, falling in between aircraft and balloons from the low

altitude side and spacecraft on the high altitude side. An advantage cited for the space shuttle was the experience gained in this region as its reentry trajectory spent much more time in this region as compared to capsules. But, this was brief compared to the indefinite time the MABHET provides. Also, simply being closer to the surface means that the resolution of sensors, such as imagers or magnetic field measuring devices, are better than spacecraft higher up and provides more complete planetary coverage than vehicles in the atmosphere rising from the surface.

4.0 Technology Roadmap

We believe that most all the propulsion system major components can be realized within 5 years. Power generation efficiency required by the MABHET concept is about 10 years away based on the previous solar power trends. The logical path to Mars flight is ground facility verification followed by LEO scale demonstration, cumulating in the Mars mission. The technology roadmap is shown in Table 2. This NIAC Phase II will show feasibility of the entire propulsion system. At the successful completion of this program, a complete propulsion system and gas source can be designed and tested in ground facilities in year 5-6 timeframe. The next step would be LEO demonstration in about 9-10 years from today onboard a primary s/c, as a secondary technology demo. Finally, in about 12 years, the technology will be ready for a Mars mission. The estimated costs to take the current technology to the point of mission insertion is <$100M. Busek has the facilities to complete the terrestrial propulsion system test, significantly reducing the cost by not requiring infrastructure. Our estimate is $10M to complete that stage. The harder to estimate cost is the preparation and LEO flight mission. We estimate the cost of this stage to fall between $50-$70M, including launch. This estimate is based on a 180kg ESPA sized spacecraft launched as a secondary payload and relatively simple mission operation, at least for the testing of the MABHET propulsion system.

The only outside technology that Busek is dependent on is the power source. Space-qualified solar cells with efficiencies very near 30% can currently be obtained from a number of venders, including Boeing Spectrolab, Emcore, and Azur Space. These high efficiency cells are all triple junction to capture more of the solar spectrum. Research-cell efficiencies have reached 43.5% this year, up from about 32% ten years ago, so we might expect that space-qualified solar cells would reach 45% or even higher ten years from now. A graph of the best cell efficiencies is shown in Figure 27, truncated from a graph published by the National Center for Photovoltaics at NREL. Other options for power source could include beamed power from a 2nd spacecraft or from Mars surface and possibly radio-isotope sources.

Table 2 Technology Roadmap to Successful Mars Flight

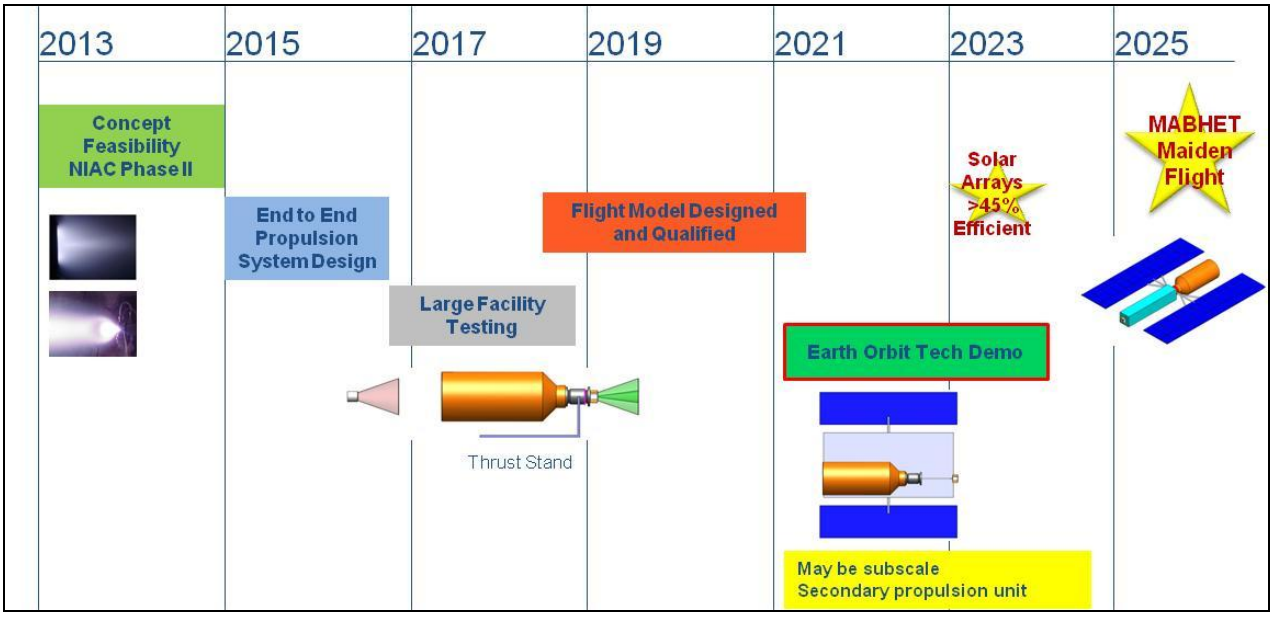

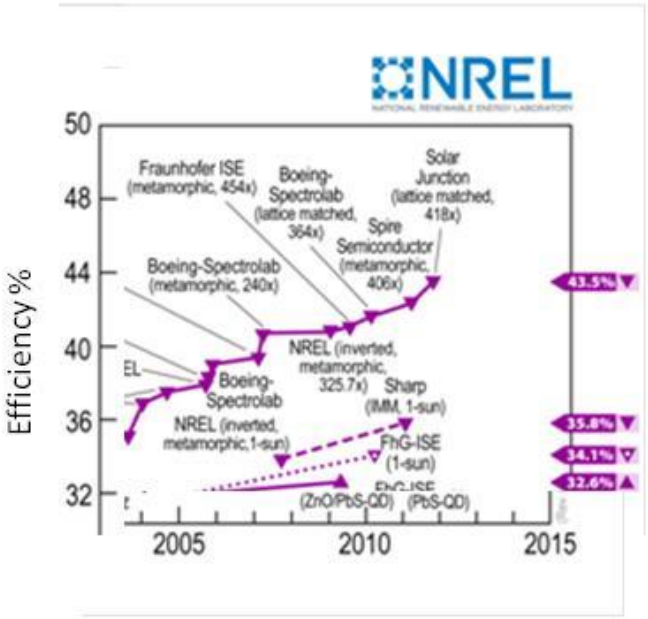

Figure 27 Truncated graph of terrestrial photovoltaic advances

5.0 Conclusions

The objective of this phase of the program was to show feasibility of a Martian atmosphere breathing Hall effect thruster (MABHET). We continued to show feasibility during this stage of the program by: measuring performance of a Busek Hall thruster with simulated Mars atmosphere, we performed additional inlet analysis that shows favorable collection, we continued overall vehicle design and analysis and began the total system analysis and possible mission potential. The thruster and atmosphere collection efficiencies are believed to be sufficient for the proposed concept. One critical parameter to be further investigated is vehicle drag in the Mars atmosphere. Additional subsystems that need work are the neutralization cathode and solar array schemes. We did not uncover any show stoppers and showed feasibility of the concept in the next 10 years. As photovoltaic arrays become more efficient, the concept becomes easier and realistic path to flight is evident.

6.0 References

1. McGowan, John, "A Mars Airplane, Wings on Mars", online white paper, www.jmcgowan.com/marsplane.html, Dec 1999.
2. Kuhl, C., "Design of a Mars Airplane Propulsion System for the Aerial Regional-Scale Environmental Survey (ARES) Mission Concept", NASA TM-2099-215700, Mar 2009.
3. Colozza, Anthony, "Preliminary Design of a Long-Endurance Mars Aircraft", NASA CR-185243, AIAA-90-2000, April 1990.
4. Clapp, M., "Dirigible Airships for Martian Surface Exploration", The Case for Mars II, 1984, p. 488-496.
5. G.A.Bird, "Molecular Gas Dynamics and the Direct Simulation of Gas Flows", ClarendonPress, Oxford, 1994.
6. "Simulated Rarefied Aerodynamics of the Magellan Spacecraft During Aerobraking," Haas, Brian L., Schmitt, Durwin A., Journal of Spacecraft and Rockets (1994), vol. 31, no. 6, pp. 980-985
7. "Rarefied Aerothermodynamic Predictions for Mars Global Surveyor," R. G. Wilmoth; D. F. Rault; F. M. Cheatwood; W. C. Engelund; R. W. Shane, Journal of Spacecraft and Rockets (1999), vol. 36, no. 3, pp. 314-322.